The effect of Ni and Sb oxide precursors, and of Ni composition, synthesis conditions and operating parameters on the activity, selectivity and durability of Sb-doped SnO_2 anodes modified with Ni

Paul Andrew Christensen*[a], Khalid Zakaria [b], Henriette Christensen[c] and Taner Yonar [d]

[a] *School of Chemical Engineering and Advanced Materials, Bedson Building, Newcastle University, Newcastle upon Tyne, NE1 7RU- Email: Paul.Christensen@newcastle.ac.uk*

Tel: +44 (0) 191 222 5472

[b] *School of Civil Engineering and Geosciences, Bedson Building, Newcastle University, Newcastle upon Tyne, NE1 7RU*

[c] *Clarizon Ltd, 17 Grange Knowe, Linlithgow, EH49 7HX*

[d] *Engineering and Architecture Faculty, Uludağ Universitesi,16059, Gorukle, Bursa, Turkey.*

Abstract

This paper reports the effect of employing Ni & Sb oxide precursors (instead of chlorides) in the preparation of Ni/Sb-SnO_2 anodes on the activity and selectivity of ozone production in 1.0M $HClO_4$. The effect of catalyst loading, Ni content in the precursor solution, furnace temperature and constant current density *vs* constant cell voltage operation is reported. The optimum composition was found to be Sn: Sb: Ni = 100: 6: 1, giving a maximum current efficiency of ca. 38% at a current density of 100 mA cm^{-2}, the latter higher than previously reported. The durability of anodes prepared using NiO and Sb_2O_3 at 550 °C during electrolysis at 100 mA cm^{-2} in 1M $HClO_4$ was found to be 200 hours, again significantly higher than Ni/Sb-SnO_2 anodes prepared using the chloride precursors at lower temperatures.

Keywords

Ozone, Ni/Sb-SnO_2, electrolysis, efficiency, activity, durability.

1. Introduction

Electrochemical ozone production (EOP) was investigated by Schönbein in the early 1800's [1]. Since then and up to 1982, Pt and PbO_2 were the only anode materials that had been investigated ([2] and references therein). Due to the poor ozone current efficiencies observed near room temperature, Pt ceased to be of interest after 1982, (with one exception, see [3]), whilst β-PbO_2 continues to be researched with respect to EOP (see, for example, [4, 5]). In recent years, a number of alternative materials have been reported as being active anodes for EOP [1] including: TiO_2 [6-8], glassy carbon [9], IrO_2-Nb_2O_5 [10, 11], tantalum oxide [12, 13], and more recently Ni/Sb-SnO_2 [14-16] and Boron Doped Diamond (BDD) [17-21].

To date, only two electrode materials have proven capable of generating ozone with efficiencies > 20% at room temperature and using solutions that do not contain expensive fluorine-containing anions: Boron Doped Diamond (BDD) [17-21] and Ni/Sb-SnO_2 [14-16, 22-27]. In general, BDD anodes are employed primarily for the oxidation of species in solution [28], *via* the production of OH radicals [29, 30], and have only shown high activity and selectivity towards the electrochemical generation of ozone in water containing no added electrolyte. It is not clear that ozone is expected to be a major product at such anodes [20].

The first report concerning the generation of ozone using Ni/Sb-SnO_2 was by Wang et al. in 2005 [14]; using a UV Vis cuvette as the electrochemical cell and a catalyst-coated 8 mm x 8 mm Ti foil anode in aqueous acid electrolyte, the authors reported current efficiencies as high as 36% at fairly low current densities (< 20 mA cm^{-2}). In 2009, Christensen and co-workers [15] reported current efficiencies of up to 50% in acid solution using 6.3 cm^2 Ni/Sb-SnO_2-coated Ti mesh (ca. 50% open area) at current densities of 30 – 40 mA cm^{-2} (geometric area). More recently, Parsa and Abbasi [25] reported a maximum ozone current efficiency of 53.7% using 6.3 cm^2 Ni/Sb-SnO_2 Ti mesh anodes in acid solution, no current density data were provided. However, the cell employed was an open

beaker, and no experimental details were given as to precisely how the ozone measurements were made. Further, on the basis of the data presented in the paper, the extinction coefficient employed by the authors for the absorption of ozone at 258 nm was 4700 M^{-1} cm^{-1}, significantly higher than the values typically employed in the literature of 3100 ± 200 M^{-1} cm^{-1} [17, 19, 31-36] and that recommended by the International Ozone Association of 3000 M^{-1} cm^{-1} [31]. Parsa and Abbasi appear to have employed the erroneous value of the extinction coefficient used by Wang et al [14]; this group later employed a value of 2900 M^{-1} cm^{-1} [37]. In addition to the incorrect extinction coefficient, the ozone absorption peaks observed by Parsa and Abbasi deviated from Gaussian shape at higher ozone concentrations [25]. Finally, the maximum of 53.7% current efficiency was seen only as a single data point, with the efficiencies tending toward steady state values < 20%. Hence, the claim by the authors of such a high efficiency is somewhat suspect.

Ozone current efficiency is generally observed to increase with current density when using non-Ni/Sb-SnO_2 anodes (*e.g.* PbO_2, Pt *etc*) [2, 9, 17-19, 38-40], at least up to a point, after which it either remains constant or decreases (most studies on the electrochemical generation of ozone employ constant current rather than constant potential or cell voltage); hence it does not seem unreasonable to postulate that the resistivity of the catalyst layer is likely to be an important factor in ozone activity. Undoped SnO_2 should be an insulator, and hence its resistivity of *ca.* 7.25 x 10^{-3} Ω cm is taken as evidence for a defect structure incorporating *eg.* O vacancies or adventitious donors [41]. SnO_2 anodes are usually doped with Sb to improve the conductivity of the electrodes (resistivities *ca.* 10^{-5} - 10^{-4} Ω cm [41, 42]), with the Sb (as Sb^{5+} [43]) replacing Sn^{4+} due to their similar ionic radii [42] and hence no change occurs in lattice parameters [44]. Resistivity initially falls with Sb doping, but then increases at higher dopant levels due to the incorporation of Sb(III) centres [45, 46] which act as trap sites for the electrons generated by Sb(V) [42]. There is some disagreement as to where the minimum resistivity occurs in Sb-doped SnO_2 anodes, e.g.: Kötz and co-workers [43] report this as

being between 4 and 9 mol.% Sb, whereas Lehmann & Widmer [47] and Chopra et al [48] suggest 0.4 – 3 mol.% Sb.

The original work on Ni/Sb-SnO_2 by Chan and co-workers [14] employed Sn, Sb and Ni precursors in the dipcoating solution at a mole ratio of 500:8:1; the actual composition of the as-made anodes has proved extremely difficult to determine due to the very small amount of Ni present [14], and remains a challenge [27]. Chan and co-workers employed ICPMS to study the composition of their anodes [14]; they found that, whilst Ni could not be detected, the ratio of Sn to Sb in the catalyst layer was 7:1, suggesting significant surface enrichment by Sb. Rumyantseva and co-workers [49] have also reported that the actual concentration of Ni in Ni-doped SnO_2 (i.e. without Sb) can deviate from that expected on the basis of the concentrations of Ni and Sn in the coating solution. However, Kotz et al. [43] using spray pyrolysis observed a 1:1 correlation between Sb in the coating solution and that in the catalyst film. In our studies, it has not proved possible to obtain reliable data using EDX, and hence we have employed XPS[1] and ToFSIMS[2] to try and detect and quantify the Ni content in our anodes. Again, it did not prove possible to detect Ni using XPS and, whilst ToFSIMS did detect the presence of Ni, the nature of the technique precluded its quantification. Thus, in the text below, reference is made only to the Ni, Sb and Sn compositions of the precursor solutions employed to produce the anodes.

[1] XPS was performed using Kratos AXIS ULTRA instrument in the Centre for Surface Chemical Analysis in Nottingham University.

[2] ToFSIMS was performed using ToF-SIMS version IV, ION-ToF GmbH, in the Laboratory of Biophysics and Surface Analysis, School of Pharmacy, Nottingham University.

The fact that the addition of very small amounts of Ni to Sb-doped SnO_2 changes the material from essentially inactive with respect to electrochemical ozone generation, to an active and highly selective ozone anode is remarkable and could not have been predicted. However, the mechanism by which O_3 evolution takes place at Ni/Sb-SnO_2 anodes remains obscure, not least as a result of the lack of quantitative analytical data on the Ni content. In one of the first papers by Wang et al. [14], the authors make some general observations on the possible effect of Ni upon the physical characteristics of SnO_2. In a later paper [50], Wang et al. present XPS data on Ni/Sb-SnO_2 anodes and state that a peak at 855.6 eV was due to the $Ni2p_{3/2}$ transition and that all the Ni in the film was in the +3 oxidation state, but the authors did not postulate a mechanism. However, in the XPS spectrum referred to, no feature is visible at the specified energy. Further, Yang and co-workers [51] report XPS data on Ni/Sb-SnO_2 anodes in which a band at 856.3 eV is evident and from which the authors conclude that all the Ni present is in the +2 state (NiO and/or $Ni(OH)_2$. Parsa and Abbasi [25] also postulate the presence of Ni(III) in their Ni/Sb-SnO_2 anodes, albeit without any experimental evidence, and they postulate a mechanism in which the Ni(III) facilitates the adsorption of molecular oxygen; water is then oxidised to OH radicals at neighbouring Sb(V) sites and these react with the adjacent adsorbed O_2 to give HO_3 radicals which are rapidly oxidised to O_3. Until definitive and quantitative analytical evidence on the composition of Ni/Sb-SnO_2 anodes to allow structure/activity correlations to be made, attempts to understand the mechanism of ozone generation at these materials will remain speculative.

Although there is a number of reports in the literature on the durability (or service life) of Ti/Sb – SnO_2 anodes [46, 52-56], there is a lack of detailed studies on the durability of Ni-doped Sb – SnO_2 anodes. In the absence of Ni, the service life of Ti/Sb – SnO_2 anodes is defined as the electrolysis time at which the anode potential increases rapidly to more than 5 V vs. the reference electrode under the operational conditions employed [27, 46]. Correa-Lozano et al. found that the service life of

Ti/Sb – SnO_2 anodes was only 12 h at 1000 A m^{-2} [46], but could be increased to 1150 h by reducing the current density to 60-200 A m^{-2} [52]. A number of papers report attempts to improve the durability of these anodes, for example: Vicent et al. [53] studied the addition of Pt to improve the service life of Ti/Sb – SnO_2 anodes at 40 mA cm^{-2} in 0.5 M K_2SO_4, and showed that a service life of 760 h could be obtained. Montilla et al [54-56] also found that the addition of trace amounts of Pt to the coating solution improved the service life of Ti/Sb – SnO_2 anodes from 300 h at 10 mA cm^{-2} in 0.5 M Na_2SO_4 solution buffered at pH = 6.9 to 990 h at 50 mA cm^{-2}. XPS data, taken together with the results of electrochemical experiments, were interpreted by Montilla and co-workers as strong evidence for the deactivation of Sb-SnO_2 *via* the formation of a passivating OH-containing layer at the SnO_2/electrolyte interface. Pt was postulated as preventing this, and hence significantly extending the service life; with added Pt, deactivation was postulated as occurring through long term attack on the Ti substrate and the formation of a passivating layer at the Ti/catalyst interface, possibly TiO_2.

To our knowledge, the only literature reports on the durability of Ni/Sb-SnO_2 anodes are by Shekarchizade and Amini [27], who reported a service life of about 600 min for the best anodes at 200 mA cm^{-2} in 0.1 M H_2SO_4, and Parsa et al. [26] who added carbon nanotubes to the coating solution and achieved up to 17 hours (compared to 3 h without the nanotubes [25]) during which the voltage increased up to 3.49 V at 53.5 mA cm^{-2} in 0.1 M $HClO_4$.

It is interesting that small changes in the composition of the precursor solution (such as adding carbon nanotubes) can have such a marked effect upon durability. Rather than explore the effect of additives, given that all the work reported on Ni/Sb-SnO_2 to date has been carried out using anodes prepared from chloride precursors and furnace temperatures $\leq 520\ ^{O}C$ [14-16, 22-27, 37, 50] it does not seem unreasonable to explore the effect of: (i) changing the Ni and Sb precursors from chlorides to

oxides (given that SnO_2 is commonly doped with Sb using Sb_2O_3 [57, 58]) and (ii) furnace temperature. The activity and selectivity of the anodes so produced were characterised in terms of: catalyst loading, Ni content in the precursor solution, furnace temperature and constant current/voltage operation. In addition, the durability of the anodes was investigated by electrolysis in 1M $HClO_4$. Further, it is clear that the development of Ni/Sb-SnO_2 anodes is still at a somewhat early stage, with some fundamental questions remaining unanswered; specifically, how durable can these materials be and what magnitude of current density can they sustain? This paper seeks to address these questions.

2. Experimental

2.1 Anode preparation and electrolytes

The catalysts were prepared according to a methodology similar to that reported previously [15] except that the Ni and Sb chlorides employed as precursors were replaced by oxides. Thus, 2.5 cm x 2.5 Ti mesh substrates were pre-treated by boiling in 10% oxalic acid for 30, then cooled down to room temperature and sonicated in Millipore water for 30 min. The Ti mesh substrate then dip-coated from ethanolic solutions of $SnCl_4.5H_2O$ (Puriss min 98%, Riedel-de Haën), Sb_2O_3 (A.C.S. reagent 99.9 +%, Aldrich) and NiO (A.C.S. reagent 99.8 %, Aldrich). $SnCl_4.5H_2O$ was dissolved in pure ethanol (ACS, > 99.5%, Sigma-Aldrich); Sb_2O_3 and NiO were first dissolved in 2.5 cm^{-3} of HCl (Puriss min 37%, Riedel-de Haën) and then added to the ethanolic $SnCl_4$ solution. The concentrations of Sn and Sb in the coating solutions were 91.40 – 93.80 at.% and 5.87 to 6.02 at.%, respectively; the Ni concentration was varied between 0.14 and 2.73 at.% corresponding to Sb:Ni mole ratios between 2.2:1 and 43.0:1. The meshes were dipped in the coating solution for 1 – 2 min, dried in oven at 100 ºC for 15 min and then calcined in furnace for further 15 min. The coating cycle (dipcoating, drying and calcining) was repeated 20 times [15, 56]). After the 20^{th} coating cycle, the anodes were calcined for 75 min. The furnace temperature was 550 ºC unless otherwise stated.

Note that an interlayer [15] was not employed, for reasons that will be covered in a subsequent paper. $HClO_4$ (Puriss, Fluka) and ethanol as well as all other chemicals were used as received without further purification. SEM and EDX analyses were carried out using a JEOL 5300LV SEM at 25 kV. In the text below, all references to the content of Ni and Sb refer to the composition of the precursor solutions.

2.2 Electrochemical cell and systems

Millipore Milli-Q water (18 MΩ cm) was used to prepare all solutions. The single pass (flow) system employed in the work reported in this paper is shown in fig. 1; the electrochemical cell [15] comprised two pyrex glass halves of oval section having ground glass flanges. The sections were clamped together on either side of a Nafion 117 membrane, sealing being achieved by means of silicone O-rings between the ground glass flanges and membrane. The volume of each half of the cell was *ca*. 100 cm^3. 1.0 M $HClO_4$ was employed as the anolyte and catholyte, which were kept separate by the membrane; both electrolyte and catholyte were supplied from a glass reservoir via polyethylene tubing (Portex 800/012/425/800 7.0 mm x 10.5 mm), with the catholyte static. The counter electrode (cathode) was a 5 cm × 5 cm platinised Ti mesh (at which hydrogen evolution occurred), and the cell voltage across the ozone anode and Pt/Ti cathode was controlled by a TTi TSX 1820P programmable DC PSU. All experiments were conducted at room temperature, 20 – 25 ºC.

The anolyte was pumped from the cell to a pyrex glass gas separator via PE tubing using a Masterflex Digital Standard Cartridge Pump (Cole-Palmer), flow rate 30 cm^3 min^{-1} unless otherwise stated. Any ozone not released from the anolyte was pumped through a 1 cm pathlength UV-Vis cell (Astranet). Nitrogen gas from a cryogenic boil-off was employed to dilute the gas exiting from the separator at a carefully-controlled rate (typically 80 cm^3 min^{-1}) using a Cole-Palmer WU series

flowmeter system and the gas phase ozone concentration monitored using a second 1 cm pathlength UV-Vis cell (Astranet). The gas-phase ozone then exhausted into a fume hood.

2.3 Durability studies

To assess the durability of the new catalyst formulation, anodes were electrolysed in a 250 cm^3 beaker at 100 mA cm^{-2} in 1M $HClO_4$ using a 5 cm x 5 cm Pt/Ti mesh as counter electrode. The cell voltage was monitored throughout the electrolyses. At intervals, the activity and selectivity of the anodes towards EOP were assessed in the glass cell in single pass mode at 100 mA cm^{-2} in 1M $HClO_4$; the total current efficiency was calculated from the gas and solution ozone absorbances at steady state (each experiment was run for *ca*. 15 – 20 minutes).

2.4 The calculation of current efficiency

For a given flow rate f (cm^3 min^{-1}) of fluid having ozone present at a concentration c and giving an absorbance A, the moles min^{-1} of ozone passing the UV Vis flow cell, $(dn/dt)_{measured}$, is:

$$(dn/dt)_{measured} = Af/1000.\varepsilon cl \qquad (1)$$

where l is the pathlength = 1 cm and ε is the molar decadic extinction coefficient of ozone = 3000 mol^{-1} dm^3 cm^{-1} [31]. Assuming a 6-electron process for ozone [39]:

$$3H_2O \rightarrow 6H^+ + 6e^- + O_3 \quad E^0 = 1.51V \textit{ vs } NHE \qquad (2)$$

dn/dt (in mol min^{-1}) assuming 100% current efficiency is:

$$(dn/dt)_{100\%} = I.60/6F \qquad (3)$$

where I is the current in Amps and F the Faraday, 96480 C mol^{-1}. Hence, the current efficiency Φ in % is given by:

$$\Phi = 100\%.(Af6F/1000.\varepsilon cl.60.I) = 0.32\ Af/I \ /\% \qquad (4)$$

and is that percentage of the total current generating ozone.

3. Results and Discussion

3.1 EDX and SEM

Typical SEM images of the electrodes prepared using the precursor solution containing 93.3, 6.0 and 0.7 at.% Sn, Sb and Ni (respectively) are shown in figs. 2(a) and (b): fig.2(a) shows an image taken of an intersection of two strands of the mesh, and fig. 2(b) of an area on a strand, both at x5000 magnification. It was generally observed that the coating on intersections exhibited a cracked morphology; an observation made by other workers [25-27] and generally attributed to thermal shock during the sudden cooling caused by withdrawing the anodes from the furnace [56], whilst the coating on strands presented a smoother appearance, suggesting a thicker coating on the intersections. The latter postulate is supported by EDX spectra of the same regions of the mesh, see figs. 2(c) & (d) and the peak assignments in table 1. The peak near 4.52 eV in fig. 2(d) may be attributed to the underlying Ti substrate, detected due to the thinner catalyst coating on the strands.

3.2 Activity and selectivity vs catalyst loading

Figure 3(a) shows a plot of catalyst loading *vs* number of dipcoats; these anodes were made to explore the effect of catalyst layer thickness on activity *etc*; each data point is the average of two anodes prepared in an identical fashion. The at.% ratio of Sn:Sb:Ni was 93.3:6.0:0.7 in the dipcoating solution. There is a fairly linear relationship between the number of coating cycles and the amount of catalyst deposited. Figure 3(b) shows (i) the corresponding current densities (measured in single pass mode) and (ii) the total (gas + solution) current efficiencies.

Figure 3(b) shows that, up to a catalyst loading of 1.0 mg cm^{-2}, current density and current efficiency increase, suggesting that there is an increase in the number of ozone and oxygen active sites, and that the ratio of the former to the latter also increases, *ie*. a greater proportion of the sites are active for ozone as the loading increases. This, in turn, suggests that the catalyst is porous such

247 that the active sites are not confined to the 'geometric' surface of the anode, and that there is,
248 perhaps, some surface enrichment by Ni, favouring ozone formation over oxygen evolution, as was
249 observed in our previous studies [16]. Figure 3(b) also shows that, after 8 dipcoats, (corresponding to
250 1.0 mg cm^{-2}), the ozone current efficiency remained constant, but the current density continued to
251 increase with catalyst loading, albeit more slowly in agreement with the work of Wang at al. [14] and
252 in contrast to Parsa et al. [25] who found that the ozone current efficiency increased with increasing
253 catalyst loading, although they prepared only 3 electrodes (according to optimum composition of
254 Wang et al. [14]) with 4, 8 and 12 coating cycles without stating the catalyst loading on the mesh.
255 Thus, above this critical loading, the number of O_2 and O_3 active sites continues to increase, but the
256 ratio of the two now remains constant.
257
258 *3.3 Comparison of constant current vs constant voltage operation*
259 Figures 4(a) and (b) show the effect of current density and cell voltage on current efficiency
260 (solution, gas and total) at constant catalyst loading; also shown in the figures are the cell voltages
261 observed at each current density or the current density observed at each cell voltage. The anode had
262 the composition Sn: Sb: Ni = 93.3 at.%: 6.0 at.%: 0.7 at.%, and comprised 10 coats (loading 1.4 mg
263 cm^{-2}). There are clearly very marked differences in terms of the current efficiencies observed
264 during the two sets of experiments. It should be noted that each data point in figs. 4(a) and (b)
265 represents a steady state measurement after $\geq$ 15 minutes at that particular cell voltage or current
266 density. To our knowledge, Parsa et al. [26] were the only research group to have studied the effects
267 of constant current density on the ozone current efficiency using co-doped Ni/Sb – SnO_2 (with and
268 without carbon nano-tube anodes), and found that the current efficiency increased up to ca. 25 mA
269 cm^{-2}, after which it declined sharply. In a separate paper, Parsa et al. [25] reported that ozone current
270 efficiency also exhibited a maximum as a function of cell voltage, an observation supported by
271 Wang et al. [14] and in contrast to our data.

Figure 4(c) compares the total current efficiencies observed as a function of current density and cell voltage (both plotted against current density imposed or observed, respectively) and the power consumption. From fig. 4(c) it can be seen that, under both constant voltage and constant current density operation, the total current efficiency rises to a maximum with increasing current density, then remains essentially constant. This transition happens near ca. 10 mA cm^{-2} at constant voltage and ca. 60 mA cm^{-2} at constant current density. Moreover, the maximum current efficiency observed is higher at constant voltage. In general, PbO_2 anodes also show increasing current efficiency up to some limiting current density (typically 1A cm^{-2}, but this value depends upon the electrolyte [2]), before levelling out and becoming independent of current density [2, 5, 38, 59-61]. There are exceptions, however; for example, Onda and co-workers [62] and Awad and Saleh [4] who observed ozone current efficiency passing through a maximum with increasing current density. Boron doped diamond (BDD) electrodes also show current efficiency both becoming independent of current density [18] and passing through a clear maximum [19]. In contrast to PbO_2, BDD and the anodes prepared in Newcastle, TiO_2 [6, 7], Pt [63], C [9] and TaO_x [12, 13] show increasing current efficiency with current density; however, this may be due to insufficient current density being applied and hence the transition in behaviour not being attained. IrO_2-Nb_2O_5 shows an onset current density for ozone evolution that varies with IrO_2 content [10].

It is not immediately clear why constant voltage should yield higher current efficiencies. As can be seen from fig. 4(c), the variation in power consumption observed is identical for the two sets of data, reflecting the fact that the same electrochemical cell and system were employed and that there is a 1:1 correlation between imposed current density and the cell voltage observed on the one hand, and imposed cell voltage and the current density observed on the other. The data in fig. 4(c) suggest that local heating effects are not observed. Early workers in electrochemical ozone generation (see [2] for an excellent review of the early work) took significant care to cool their anodes

297 to avoid heating as it was shown that current efficiency generally increased as temperature was
298 decreased [64] and references therein, [9, 63, 65], with temperatures down to -60 ºC being found to be
299 particularly effective [9, 65]. Lash and co-workers [65] showed that high current densities resulted in
300 local heating of the anode which obscured the actual effect of such current densities on current
301 efficiency; the authors were able to deconvolute the effect of local heating by careful cooling of the
302 anode. However, all the above workers employed significantly higher current densities than those
303 reported in this paper.
304
305 *3.4 Optimisation of the Ni concentration*
306 Figure 5(a) shows the effect of Ni concentration in the dipcoating solution on the current density
307 and current efficiency. Each anode comprised 8 dipcoats with mean loadings of 0.94 ± 0.10 mg cm^{-2}
308 , and each datapoint was the average of two 15 – 20 minute experiments with the ozone efficiency
309 measured at steady state.
310
311 As may be seen from the figure, the current density remains essentially constant as the
312 concentration of Ni is increased in the catalyst to *ca*. 1.04 at.%; however, there is a 45% increase in
313 current efficiency over this range, *ie*. from 20 to 29%. This suggests relatively little change in the
314 total number of active sites but a very marked increase in the ratio of O_3 to O_2 sites, in line with the
315 postulated key role of Ni in the O_3 active site. At higher concentrations, the current efficiency
316 appears to remain constant, or decrease slightly, whereas the current density shows a sharp decline.
317 The data in fig. 5(a) are in broad agreement with the work of Shekarchizade and Amini [27] and Wang
318 et al. [50]; the former found that ozone current efficiency increases with increasing Ni in the coating
319 solution up to an optimum, although they observed the optimum Ni concentration to be ca. 0.2 at.%
320 (and an optimum Sb concentration of *ca*. 2 at.%). Wang et al. observed an optimimum efficiency at
321 a concentration of 0.71 at.% Ni in the coating solution.

Interpreting the data in fig. 5(a) poses a challenge as, as well as the uncertainty regarding the actual content of Ni in the catalyst films, whilst there is a wealth of literature on the physicochemical characteristics of Ni-doped SnO_2 due to potential application in varistors [66] and solid state gas sensors [49, 67], apart from the brief treatment in Shekarchizade and Amini [27] there is no such data in the literature to our knowledge on Ni and Sb-doped SnO_2. Thus, it does not seem unreasonable to use the literature on Ni doped SnO_2 as a starting point; on this basis, the significant increase in current efficiency up to 1.04 at.% may simply reflect the replacement of the Sn by Ni (due to their similar size, *ie*. 0.072 nm and 0.071 nm, respectively [49, 66, 67]) throughout the catalyst, and hence the increase in active ozone sites at the electrode/electrolyte interface. The constant current density is due to the fact that the minimum in resistivity for Sb-doped SnO_2 is fairly broad [48].

From the Ni-doped SnO_2 literature, it is clear that the physicochemical properties of SnO_2 undergo major changes around 1 at.% Ni [49, 66, 67]. In particular, Aragón and co-workers [67] employed Raman spectroscopy and have shown that, at Ni $\leq$ 1 mol.%, the Ni primarily forms a solid solution with SnO_2 with some segregation to the surface, but at $\geq$ 2%, the latter process dominates. It does not seem unreasonable to postulate that the decrease in current density at Ni > 1.04 at.% is due to the resistivity rising with increasing Ni (moving out of the minimum resistivity due to the increased doping by Ni on top of the effect of the fixed Sb doping) and to an excessive surface concentration of Ni. Figure 5(b) shows current/voltage plots for the anodes with 0.35, 1.04 and 1.72 at.% Ni: it can be seen from the figure that, whilst the plots for 0.35 and 1.04 at.% Ni are similar, with the latter giving a slightly higher current at 2.7V, the plot for 1.72 at.% Ni is significantly more resistive as well as giving lower current, in agreement with the discussion above. In contrast, Shekarchizade and Amini [27] and Wang et al [50] both report that the resistance of Ni/Sb-SnO_2 anodes increases with increasing content (rather than passing through a maximum) and attribute the decline in efficiency after the maximum to this increase.

3.5 The effect of furnace temperature

Figure 6(a) shows plots of catalyst loading vs furnace temperature for Ni/Sb-SnO_2 films having (i) 0.7 at.% and (ii) 1.4 at.% Ni, 8 coats. Each datapoint is the average of the masses of three anodes prepared in an identical manner; the ranges of the loading values are shown on the plot. As may be seen, the furnace temperature seemed to affect the loading of catalysts in a way that depended very little upon the concentration of Ni. Figure 6(b) shows the current density data for the experiments on the anodes shown in fig. 6(a); whilst there is little variation with furnace temperature for the anodes with 1.4 at.%, the anodes with 0.7 at.% show a clear maximum in current density at 460 ºC. This maximum is reflected in the plot of total current efficiency *vs* furnace temperature in fig. 6(c) which also shows a clear maximum at 460 ºC. All the anodes had loadings above the *ca*. 1.0 mg cm^{-2} threshold for constant current efficiency; furthermore, the catalyst loadings of the anodes decreased as furnace temperature increased. This supports the postulate that current density is an important parameter in determining current efficiency. However, the anodes with 1.4 at.% also show a clear maximum in current efficiency, without this being mirrored in the plot of current density, or that showing the variation in catalyst loading; in addition, the current efficiency remains constant in fig. 5(a) at higher Ni content whilst the current density decreases sharply. Hence current density cannot be the ***only*** factor governing current efficiency. This in agreement with Rufino et al. [68] and Da Silva et al. [69] who reported that ozone current efficiency is affected by temperature, real current density (i.e taking into account electrochemically active surface area), electrode and electrolyte composition.

3.6 Durability

The anodes prepared at 460 ºC clearly show higher current efficiencies than those prepared at 550 ºC, albeit comparable current densities. The question then arises as to whether furnace temperature affects durability and, if so, in what way? Figure 7 shows the results of a durability study carried

372 out as described in section 2.3 on anodes prepared from the same dipcoating solution (containing Ni
373 and Sb oxides as precursors, and at 550 °C) in an identical manner. The anode failed after *ca*. 200
374 hours electrolysis in 1M $HClO_4$ at 100 mA cm^{-2}. A second anode prepared in an identical manner
375 to that in fig. 7 also failed after 200 hours electrolysis. Anodes prepared at 390 ºC and 460 ºC
376 failed within *ca*. 40 hours; this may be related to the fact that the crystallinity of SnO_2 increases
377 with furnace temperature from 450 °C to 550 °C [46]. Nevertheless, even the latter lifetime was a
378 significant improvement on the durability of the anodes prepared using all-chloride precursors, as
379 well as on the lifetime of anodes reported in the literature. Thus, Shekarchizade and Amini [27]
380 prepared their anodes at 520 °C and have shown that the Ni and Sb concentrations in the coating
381 solution are key factors affecting the service life of the anodes; however, the highest service life the
382 authors observed was ca. 600 min at a Sb concentration of ca. 12 % and Ni concentration of ca.
383 0.2 %, but the authors reported that this composition did not give the highest current efficiency.
384 The authors reported that anodes having the optimum composition with respect to current efficiency
385 (2% Sb and 0.2% Ni) showed a service life of only 300 min. The very significant difference
386 between the service life of the anodes discussed in this paper and those studied by Shekarchizade
387 and Amini is most likely related to the use of Sb_2O_3 and NiO instead of the chloride salts and
388 possibly the slightly higher furnace temperature, and this is under further investigation.
389
390 Again, of necessity, using the literature on Sb-SnO_2 anodes, the deactivation of Ni/Sb-SnO_2
391 electrodes could be due, in broad terms, to one or all of the following processes: (1) physical loss of
392 catalyst due (i) spallation (stress cracking from formation of TiO_2 under the coating [46] and/or (ii)
393 corrosion (etching away of the surface as observed by Foller and Tobias [64]); (2) formation of a
394 'passivating' layer at the catalyst/electrolyte interface [43, 54-56]. The dissolution of Ni from Ni(II)O
395 could be a very real problem [70]. However, according to Pourbaix [71] and the potentials of the various Ni
396 species [70-72] (note: reference [70] gives the Ni(III) species as $Ni(OH)_3$; this is more likely to be NiOOH[73])

at pH 0 (the typical pH of the experiments reported in this paper) and at a cell voltage of 2.7 V *vs* the counter electrode (which evolves H_2), Ni would be expected to be in the form of the stable Ni(III) species which (as was discussed above) may also be the active site for ozone evolution.

At the end of the durability experiment shown in fig. 7 (and the repeat with the second anode) powder was noted in the bottom of the beakers; SEM images of these powders suggested that they were catalyst that had spalled off the Ti mesh, see fig. 8. The loss of catalyst was supported by EDX spectra of the meshes which showed only Ti present. This suggests that failure was due to relatively rapid, complete spalling of the catalyst, either due to stress or to the oxidation of the underlying Ti to TiO_2.

4. Conclusions

The use of a slightly higher furnace temperature and/or Ni and Sb oxides as precursors (instead of chlorides) significantly increases both the current density that Ni/Sb-SnO_2 anodes are able to sustain and their durability. The former is more than doubled (the highest current densities yet reported), and durability increased from a few tens of hours to 200 hours (also the highest reported). Whilst the maximum current efficiency of ca. 38% is not as high as the 50% observed using anodes made from chloride precursors, the ca. 25 – 30% routinely observed is comparable.

The dipcoating procedure results in thicker catalyst layers at the intersection of strands of mesh than on the strands themselves and the morphologies of the layers at these positions are different. Overall, catalyst loading increases linearly with the number of dipcoating cycles, forming a porous layer, with the active, Ni-containing sites not confined to a two-dimensional surface up to *ca*. 1 mg cm^{-2}.

Nickel is essential for the generation of ozone, but excessive amounts reduce both current efficiency and current density, the latter due to increased resistance; the optimum appears to be 1.04 at.% Ni.

Furnace temperature has a marked effect upon current efficiency, with a temperature of 460 °C being optimum; however, this (and lower) temperatures result in poor durability compared to those anodes prepared at 550 °C.

A future paper will report the fact that, with further modification of the precursor solutions, durability can be increased to more than 600 hours.

5. Acknowledgements

KZ would like to thank Damascus University, Syria, for sponsorship and TY would like to thank Uludağ Universitesi for funding (OUAP-M2012-10).

Peak /eV	**Relative intensity Sb_2O_5**	**Assignment**	**Peak /eV**	**Assignment**	**Typical relative intensity Ni/Sb-SnO_2**
3.62	1.00	Sb	3.48	Sn	1.00
3.88	0.39		3.70	Sn+Sb	0.55
4.11	0.12		3.93	Sn+Sb	0.20
4.37	0.07		4.15	Sn+Sb	0.09
			4.52	Ti	

435

436 Table 1 Assignments and relative peak intensities of the various features in the EDX spectra of

437 Ni/Sb-SnO_2 anodes [16].

6. **References**

1. P. A. Christensen, T. Yonar, and K. Zakaria, *Ozone Science and Engineering,* **In Press** (2012).
2. P. C. Foller and C. W. Tobias, *Journal of the Electrochemical Society,* **129** (3), 506-515 (1982).
3. F. Okada and K. Naya, *J. Electrochem. Soc.,* **156** (8), E125-E131 (2009).
4. M. I. Awad and M. M. Saleh, *Journal of Solid State Electrochemistry,* **14** (10), 1877-1883 (2010).
5. L. M. Da Silva, D. V. Franco, L. G. Sousa, and I. C. Goncalves, *Journal of Applied Electrochemistry,* **40** (4), 855-864 (2010).
6. K. Kitsuka, K. Kaneda, M. Ikematsu, M. Iseki, K. Mushiake, and T. Ohsaka, *Electrochimica Acta,* **55** (1), 31-36 (2009).
7. K. Kitsuka, K. Kaneda, M. Ikematsu, M. Iseki, K. Mushiake, and T. Ohsaka, *Journal of the Electrochemical Society,* **157** (2), F30-F34 (2010).
8. J. E. Graves, D. Pletcher, R. L. Clarke, and F. C. Walsh, *Journal of Applied Electrochemistry,* **22** (3), 200-203 (1992).
9. P. C. Foller and G. H. Kelsall, *Journal of Applied Electrochemistry,* **23** (10), 996-1010 (1993).
10. M. H. P. Santana, L. A. De Faria, and J. F. C. Boodts, *Electrochim. Acta,* **49** (12), 1925-1935 (2004).
11. M. H. P. Santana, L. A. De Faria, and J. F. C. Boodts, *J. Appl. Electrochem.,* **35** (9), 915-924 (2005).
12. K. Kaneda, M. Ikematsu, Y. Koizumi, H. Minoshima, T. Rakuma, D. Takaoka, and M. Yasuda, *Electrochemical and Solid State Letters,* **8** (6), J13-J16 (2005).
13. K. Kaneda, M. Ikematsu, K. Kitsuka, M. Iseki, H. Matsuura, T. Higuchi, T. Hattori, T. Tsukamoto, and M. Yasuda, *Japanese Journal of Applied Physics Part 1-Regular Papers Brief Communications & Review Papers,* **45** (8A), 6417-6419 (2006).
14. Y. H. Wang, S. A. Cheng, K. Y. Chan, and X. Y. Li, *Journal of the Electrochemical Society,* **152** (11), D197-D200 (2005).
15. P. A. Christensen, W. F. Lin, H. Christensen, A. Imkum, J. M. Jin, G. Li, and C. M. Dyson, *Ozone-Science & Engineering,* **31** (4), 287-293 (2009).
16. P. A. Christensen, K. Zakaria, and T. P. Curtis, *Ozone-Science & Engineering,* **34** (1), 49 - 56 (2012).
17. K. Arihara, C. Terashima, and A. Fujishima, *Electrochemical and Solid State Letters,* **9** (8), D17-D20 (2006).
18. K. Arihara, C. Terashima, and A. Fujishima, *Journal of the Electrochemical Society,* **154** (4), E71-E75 (2007).
19. A. Kraft, M. Stadelmann, M. Wunsche, and M. Blaschke, *Electrochemistry Communications,* **8** (5), 883-886 (2006).
20. P. A. Michaud, M. Panizza, L. Ouattara, T. Diaco, G. Foti, and C. Comninellis, *Journal of Applied Electrochemistry,* **33** (2), 151-154 (2003).
21. Y. Nishiki, N. Kitaori, and K. Nakamuro, *Ozone Science and Engineering,* **33** (2), 114-120 (2011).
22. S. A. Cheng and K. Y. Chan, *Electrochemical and Solid State Letters,* **7** (3), D4-D6 (2004).
23. P. A. Christensen, and Imkum, A., *Ozone-Science & Engineering,* **33** (5), 389-395 (2011).
24. Y. H. Wang, S. Cheng, and K.-Y. Chan, *Green Chemistry,* **8** (6), 568-572 (2006).
25. J. B. Parsa and M. Abbasi, *J Solid State Electrochem,* **16** 1011 - 1018 (2012).
26. J. B. Parsa, M. Abbasi, and A. Cornell, *Journal of The Electrochemical Society,* **159** (5), D265 - D269 (2012).

27. H. Shekarchizade and K. M. Amini, *International Journal of Electrochemistry*, **2001** (1 - 13), 1 (2011).
28. C. A. Martinez-Huitle and E. Brillas, *Applied Catalysis B-Environmental*, **87** (3-4), 105-145 (2009).
29. A. Kapalka, G. Foti, and C. Comninellis, *Electrochimica Acta*, **54** (7), 2018-2023 (2009).
30. M. Panizza and G. Cerisola, *Electrochimica Acta*, **51** (2), 191-199 (2005).
31. A. Nemes, I. Fabian, and G. Gordon, *Ozone-Science & Engineering*, **22** (3), 287-304 (2000).
32. K. Rakness, G. Gordon, B. Langlais, W. Masschelein, N. Matsumoto, Y. Richard, C. M. Robson, and I. Somiya, *Ozone Sci. Eng.*, **18** 209 – 229 (1996).
33. J. Hoigne and H. Bader, *Water Res.* , **10** 377 – 386 (1976).
34. R. E. Buhler, J. Staehelin, and J. Hoigne´, *J. Phys. Chem.*, **99** 2560 – 2564 (1984).
35. K. Sehested, H. Corfitzen, J. Holcman, and E. J. Hart, *J. Phys. Chem. A*, **102** 2667 – 2672 (1998).
36. M.-O. Buffle, J. Schumacher, E. Salhi, M. Jekel, and U. V. Gunten, *Water Res.*, **40** 1884 - 1894 (2006).
37. Y. Cui, Y. Wang, B. Wang, H. Zhou, K. Y. Chan, and Z. Y. Li, *J. Electrochem. Soc.* , **156** (4), E75 - E80 (2009).
38. S. Stucki, G. Theis, R. Kotz, H. Devantay, and H. J. Christen, *Journal of the Electrochemical Society*, **132** (2), 367-371 (1985).
39. S. Stucki, H. Baumann, H. J. Christen, and R. Kotz, *Journal of Applied Electrochemistry*, **17** (4), 773-778 (1987).
40. P. Tatapudi and J. M. Fenton, *Journal of the Electrochemical Society*, **141** (5), 1174-1178 (1994).
41. S. Shanthi, C. Subramanian, and P. Ramasamy, *Journal of Crystal Growth*, **197** (4), 858-864 (1999).
42. K. Y. Rajpure, M. N. Kusumade, M. N. Neumann-Spallart, and C. H. Bhosale, *Materials Chemistry and Physics*, **64** (3), 184-188 (2000).
43. R. Kotz, S. Stucki, and B. Carcer, *Journal of Applied Electrochemistry*, **21** (1), 14-20 (1991).
44. E. Shanthi, V. Dutta, A. Banerjee, and K. L. Chopra, *Journal of Applied Physics*, **51** (12), 6243-6251 (1980).
45. B. Correa-Lozano, C. Comninellis, and A. DeBattisti, *Journal of the Electrochemical Society*, **143** (1), 203-209 (1996).
46. B. Correa-Lozano, C. Comninellis, and A. DeBattisti, *Journal of Applied Electrochemistry*, **27** (8), 970-974 (1997).
47. H. W. Lehmann and R. Widmer, *Thin Solid Films*, **27** (2), 359-368 (1975).
48. K. L. Chopra, S. Major, and D. K. Pandya, *Thin Solid Films*, **102** (1), 1-46 (1983).
49. M. N. Rumyantseva, O. V. Safonova, M. N. Boulova, L. I. Ryabova, and A. M. Gas'kov, *Russian Chemical Bulletin*, **52** (6), 1217-1238 (2003).
50. Y. H. Wang, K. Y. Chan, X. Y. Li, and S. K. So, *Chemosphere* **65** 1087 – 1093 (2006).
51. S. Y. Yang, Y. S. Choo, S. Kim, S. K. Lim, J. Lee, and H. Park, *Applied Catalysis B: Environmental* **111– 112** 317 – 325 (2012).
52. L. Lipp and D. Pletcher, *electrochimica Acta*, **42** 1091 - 1099 (1997).
53. F. Vicent, E. Morallon, C. Quijada, J. L. Vazquez, A. Aldaz, and F. Cases, *JOURNAL OF APPLIED ELECTROCHEMISTRY*, **28** 607 - 612 (1998).
54. F. Montilla, E. Morallon, A. De Battisti, S. Barison, S. Daolio, and J. L. Vazquez, *Journal of Physical Chemistry B*, **108** (41), 15976-15981 (2004).
55. F. Montilla, E. Morallon, A. De Battisti, A. Benedetti, H. Yamashita, and J. L. Vazquez, *Journal of Physical Chemistry B*, **108** (16), 5044-5050 (2004).
56. F. Montilla, E. Morallon, A. De Battisti, and J. L. Vazquez, *Journal of Physical Chemistry B*, **108** (16), 5036-5043 (2004).

57. Y. Feng, Y. Cui, B. Logan, and Z. Liu, *Chemosphere* **70** 1629 – 1636 (2008).
58. Y. Cui, Y. Feng, J. Liu, and N. Ren, *Journal of Hazardous Materials*, **239 - 240** 225 - 232 (2012).
59. Y. Beaufils, C. Comninellis, and P. Bowen, *Preparation and characterisation of Ti/IrO2/Pb electrodes for ozone production in a SPE electrochemical cell*, p. 191-200 (1999).
60. P. Tatapudi and J. M. Fenton, *Journal of the Electrochemical Society*, **140** (12), 3527-3530 (1993).
61. S. D. Han, J. D. Kim, K. S. Myung, R. K. Rana, and K. C. Singh, *Indian Journal of Chemical Technology*, **13** (2), 156-161 (2006).
62. K. Onda, T. Ohba, H. Kusunoki, S. Takezawa, D. Sunakawa, and T. Araki, *Journal of the Electrochemical Society*, **152** (10), D177-D183 (2005).
63. J. D. Seader, and Tobias, C. W., *Industrial and Engineering Chemistry*, **44** (9), 2207 - 2211 (1952).
64. P. C. Foller and C. W. Tobias, *Journal of the Electrochemical Society*, **129** (3), 567-570 (1982).
65. E. I. Lash, Hornbeck, R. D., Putnam, G. L., and Boleter, E. D. , *Journal of Electrochemical Society*, **98** (4), 134-137 (1951).
66. J. F. Wang, H. C. Chen, W. X. Wang, W. B. Su, and G. Z. Zang, *Materials Science and Engineering B-Solid State Materials for Advanced Technology*, **99** (1-3), 465-469 (2003).
67. F. H. Aragon, J. A. H. Coaquira, P. Hidalgo, S. W. da Silva, S. L. M. Brito, D. Gouvea, and P. C. Moraisa, *Journal of Raman Spectroscopy*, **42** (5), 1081-1086 (2010).
68. E. C. G. Rufino, M. H. P. Santana, L. A. De Faria, and L. M. Da Silva, *Chemical Papers*, **64** (6), 749 - 757 (2010).
69. L. M. Da Silva, L. A. De Faria, and J. F. C. Boodts, *Electrochimica Acta*, **48** 699 - 709 (2003).
70. A. J. Bard, R. Parsons, and J. Jordan, *Standard Potentials in Aqueous Solution*, p. 339, International Union of Pure and Applied Chemistry, New York and Basel (1985).
71. M. Pourbaix, *Atlas of Electrochemical Equilibria in Aqueous Solutions*, p. 342, National Association of Corrosion Engineering, Texas (1974).
72. D. D. Wagman, W. H. Evans, V. B. Parker, R. H. Schumm, I. Halow, S. M. Bailey, K. L. Churney, and R. L. Nuttall, *Journal of Physical and Chemical Reference Data*, **11** (2), 1807-1812 (1982).
73. F. A. Cotton, and G. Wilkinson, C. A. Murillo and M. Bochmann, *Advanced Inorganic Chemistry*, p. 854, Wiley - VCH, Toronto (1999).

Figure captions

1. The single pass (flow) system for generating ozone in the glass cell, see text for details.

2. Typical SEM images (x5000, bar = 5 μm) of two areas of a Ni/Sb-SnO_2 coated Ti mesh (a) the intersection of two strands of the mesh, and (b) a strand. (c) & (d) EDX spectra of the same regions of the electrode in figs. 2(a) and (b): (c) the intersection and (d) the strand. The coating solution employed to prepare the anode contained Sn, Sb and Ni in the mole ratio 93.3: 6.0: 0.7, the 2.5 cm x 2.5 cm Ti mesh was dipcoated 18 times giving a catalyst loading of 2.5 mg cm^{-2}.

3. (a) Plot of catalyst loading *vs* number of dipcoats. Each datapoint is the average of two anodes prepared by the same method. (b) Plots of (i) current density and (ii) current efficiency for the anodes in fig. 3(a). Current densities were measured at a cell voltage of 2.7V in single pass mode at an anolyte (1M $HClO_4$) flow rate of 30 cm^3 min^{-1} in the glass cell, and total current efficiencies were calculated from the current passed and the gas & dissolved ozone absorbances. The coating solution contained Sn, Sb and Ni in the mole ratio 93.3: 6.0: 0.7.

4. Plots of (i) total (gas+solution) current efficiency and (ii) cell voltage or current density for experiments carried out in the glass cell using single pass mode in 1M $HClO_4$ at (a) constant current density and (b) constant cell voltage. The anolyte flow rate was 60 cm^3 min^{-1}, and the anode was 10 coats, 1.44 mg cm^{-2}, with a Sb:Ni composition of 6.0 at.%:0.7 at.%. Each data point was measured once the system had reached steady state, typically ca. 15 minutes from the start of each experiment. (c) Plots of current efficiency and power consumption (cell

voltage x current) for the experiments in (a) and (b): (i) & (iv) at constant cell voltage, (ii) & (iii) constant current density.

5. Plots of (a) current density and total current efficiency *vs* nickel concentration in the catalyst coating solution (at.%) for Ni/Sb-SnO_2 anodes with 6 at.% Sb. Each anode comprised 8 dipcoats, 0.94 ± 0.10 mg cm^{-2}, and each data point was the average of two distinct, *ca*. 15 minute experiments using two anodes of identical composition in the glass cell at 2.7V using 1M $HClO_4$ as anolyte and catholyte in single pass mode measuring both gas and dissolved ozone. Anolyte flow rate 30 cm^3 min^{-1}. (b) Current/voltage plots for the Ni/Sb-SnO_2 anodes in (a) having (i) 0.35, (ii) 1.04 and (iii) 1.72 at. % Ni in the coating solution. The cell voltage was stepped up from 2 to 3.0V and the current measured after ca. 1 minute for each step; the voltage was then stepped down from 3.0V and the measurements repeated.

6. Plots of (a) catalyst loading, (b) current density and (c) total current efficiency as a function of furnace temperature for Ni/Sb-SnO_2 anodes having (i) 0.7 at.% and (ii) 1.4 at.% Ni, 8 coats. Each datapoint is the average of two experiments (15 minutes) using three anodes prepared in an identical manner. The current densities and ozone efficiencies were measured at 2.7V in single pass mode using the glass cell and 1M $HClO_4$ as anolyte and catholyte; anolyte flow rate 30 cm^3 min^{-1}.

7. Plots of (i) total current efficiency and (ii) cell voltage taken at intervals during a durability experiment in which an anode was electrolysed in a 250 cm^3 beaker at 100 mA cm^{-2} in 1M $HClO_4$ using a 5 cm x 5 cm Pt/Ti mesh as counter electrode. The cell voltage was monitored throughout the electrolysis. At intervals, the activity and selectivity of the anode were assessed in the glass cell in single pass mode at 100 mA cm^{-2} in 1M $HClO_4$; the total current

efficiency was calculated from the gas and solution ozone absorbances at steady state (each experiment was run for *ca*. 15 – 20 minutes). The anode was prepared from a coating solution containing 93.3 at.% Sn, 6.0 at.% Sb and 0.7 at.% Ni, 20 dipcoats to give a loading of 2.70 ± 0.05 mg cm^{-2}, furnace 550 ºC.

8. SEM image of the powder collected from the bottom of the cell after the durability study depicted in fig. 7. Magnification x 250: bar = 100 μm.

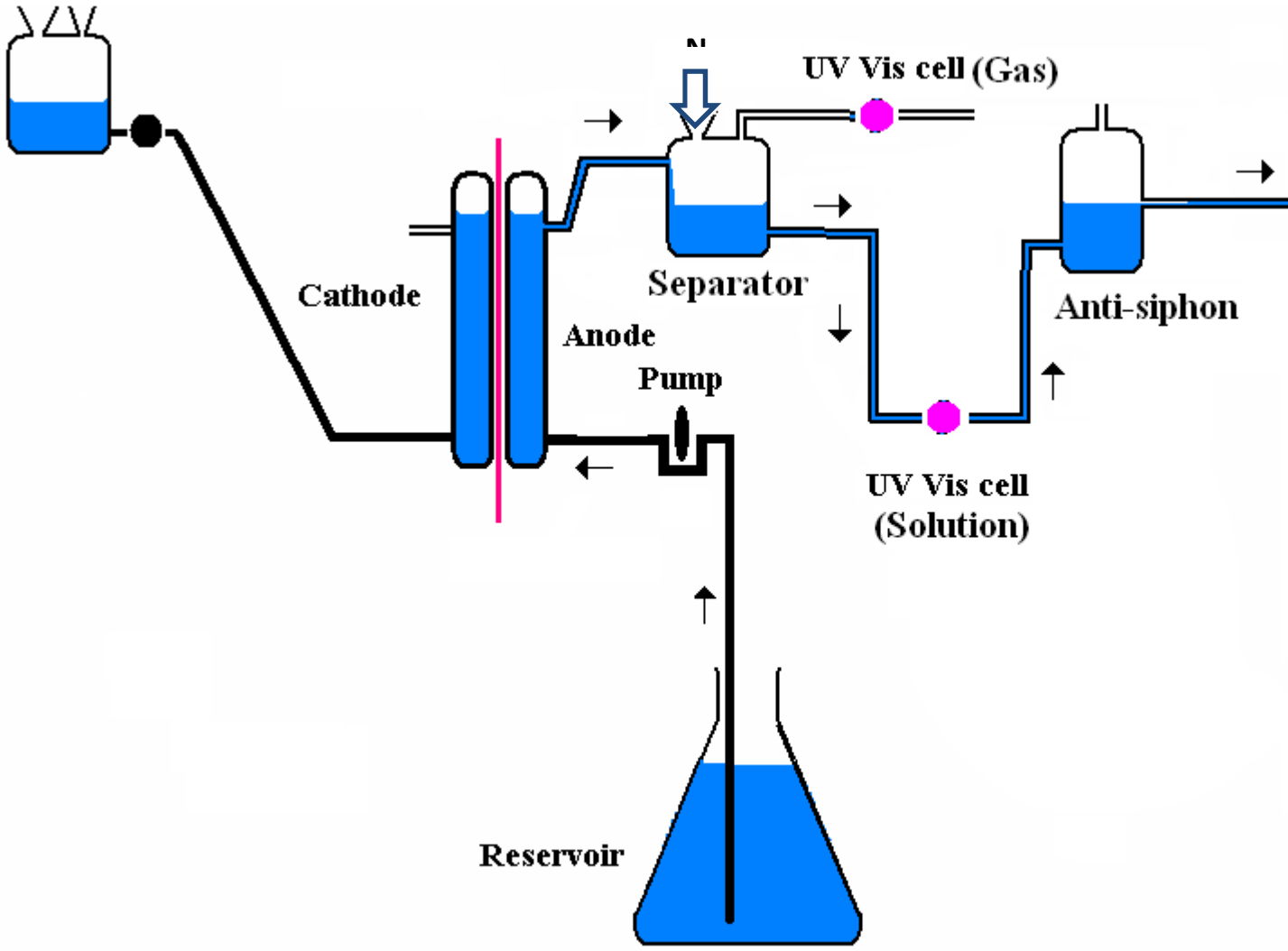

630

631 Figure 1

632

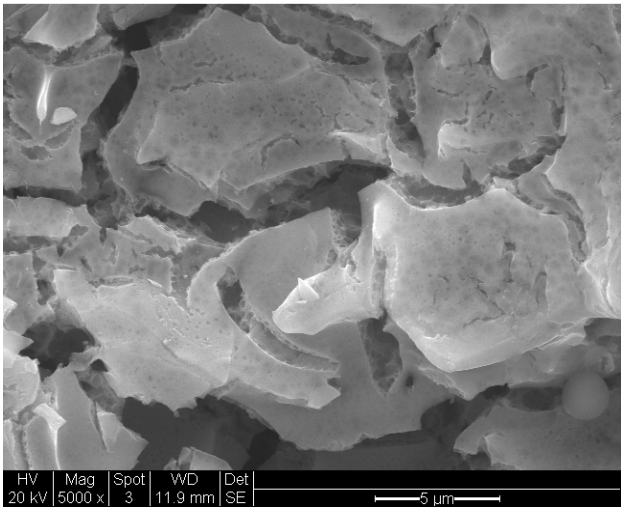

633

634 Figure 2(a)

635

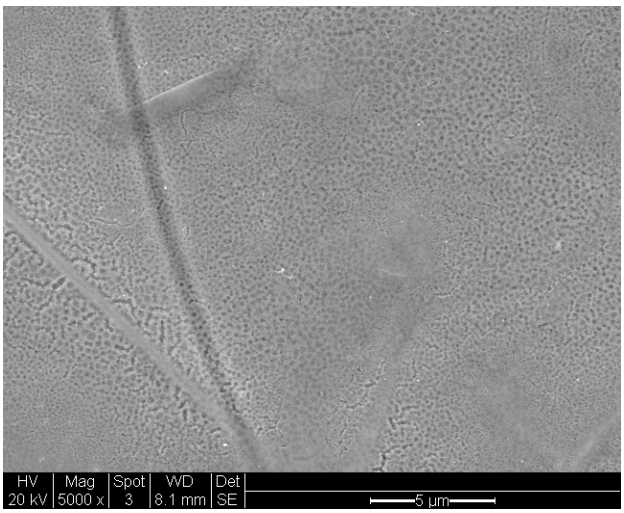

Figure 2(b)

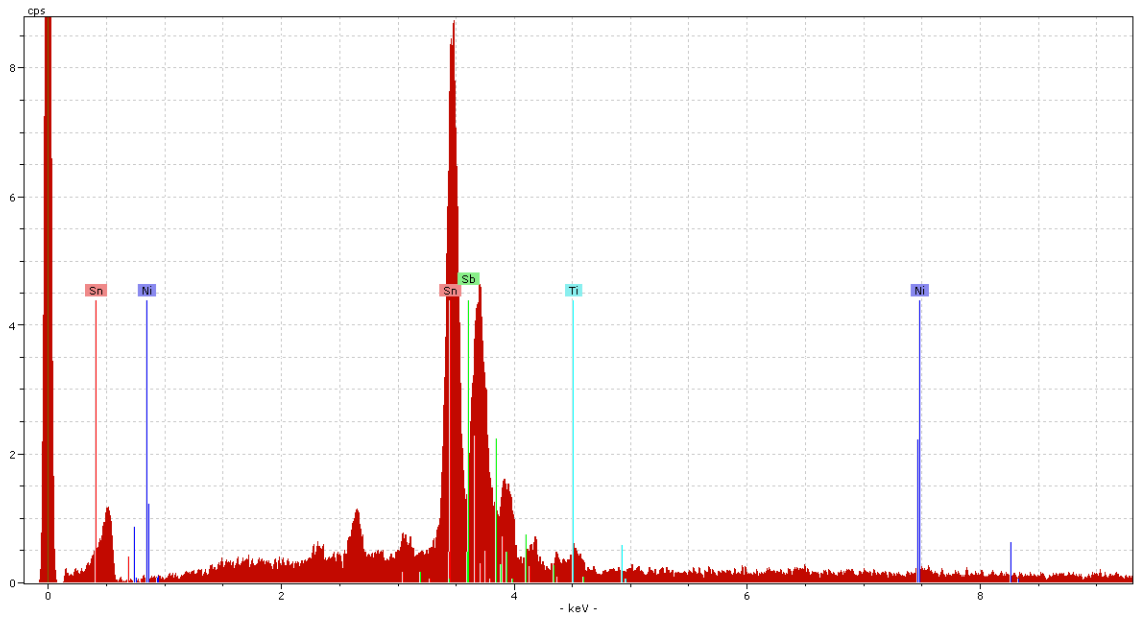

Figure 2(c)

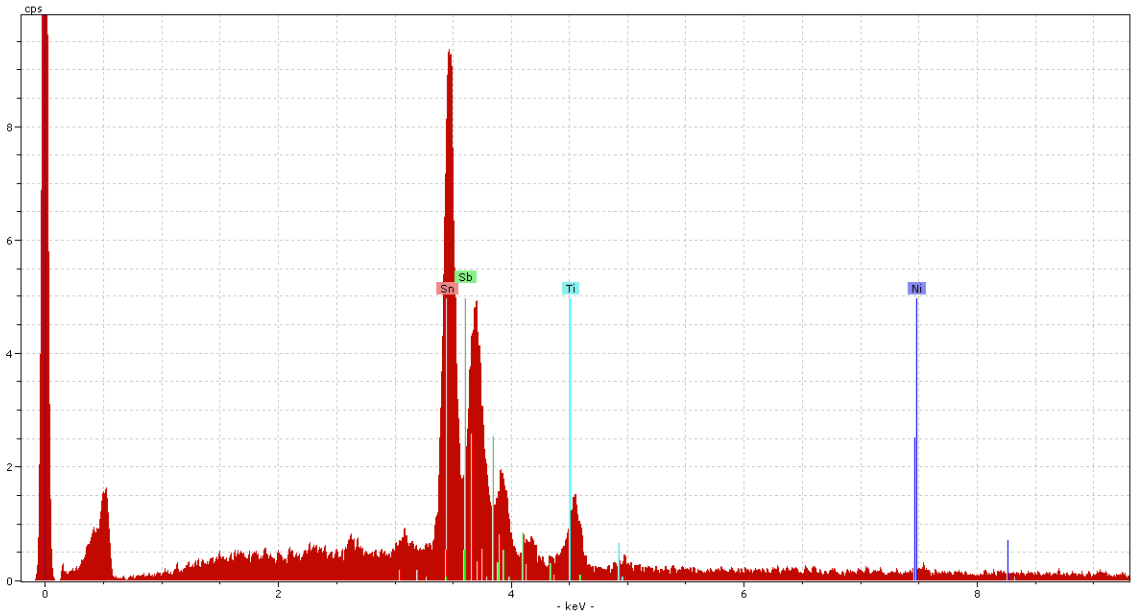

641

642 Figure 2(d)

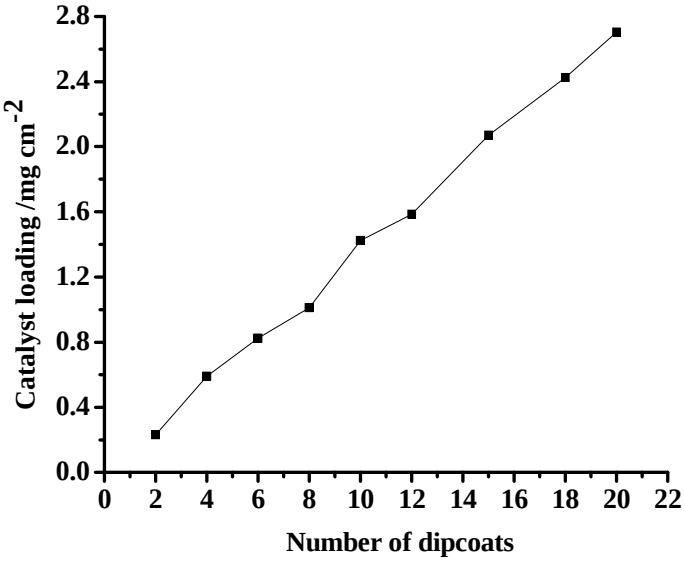

643

644 Figure 3(a)

645

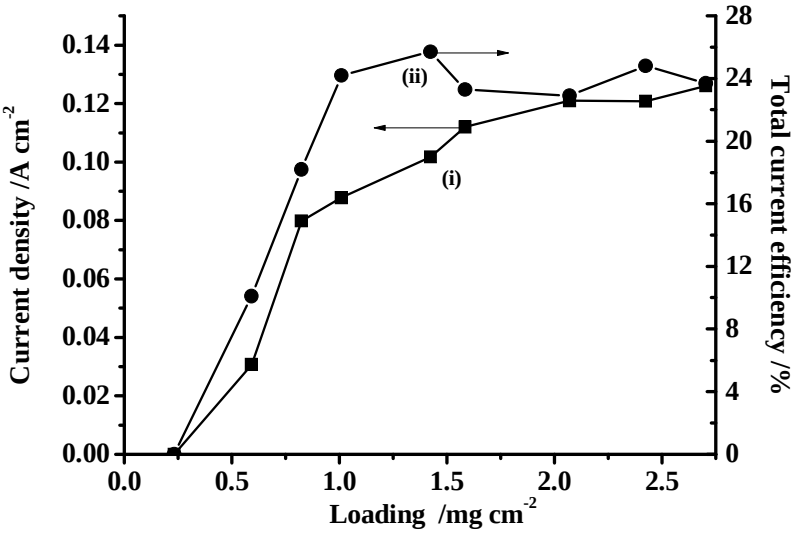

646

647 Figure 3(b)

648

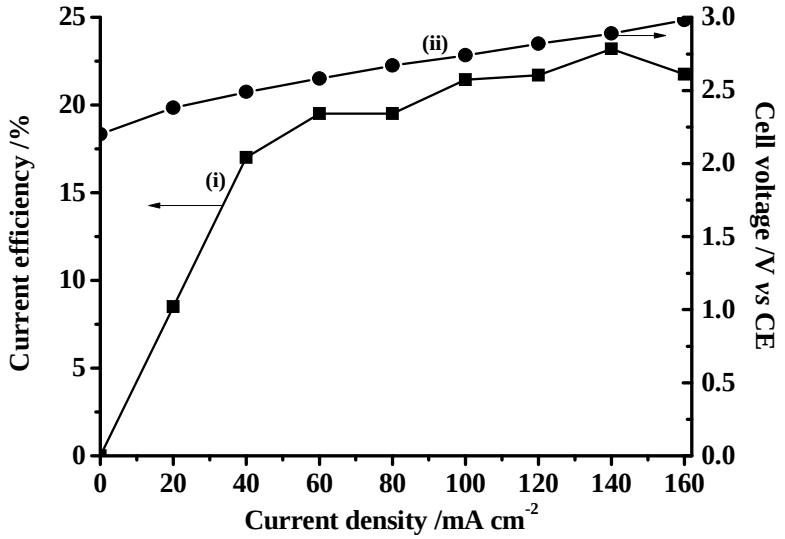

649

650 Figure 4(a)

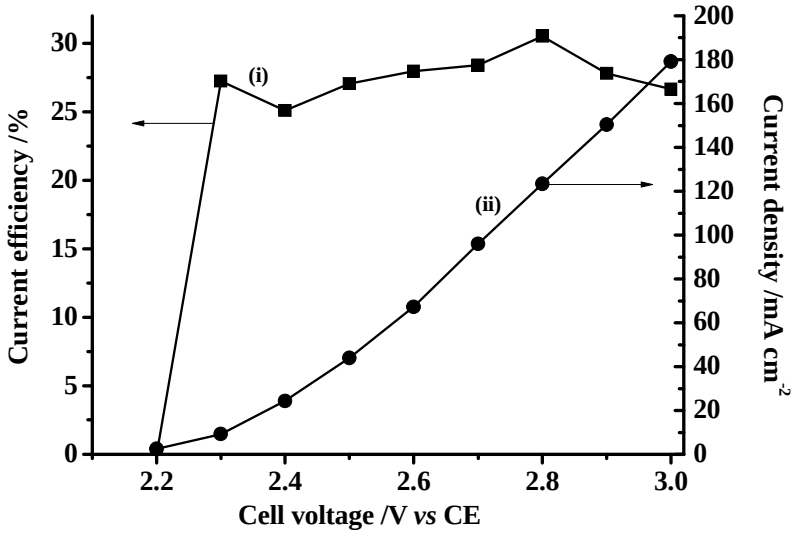

651

652 Figure 4(b)

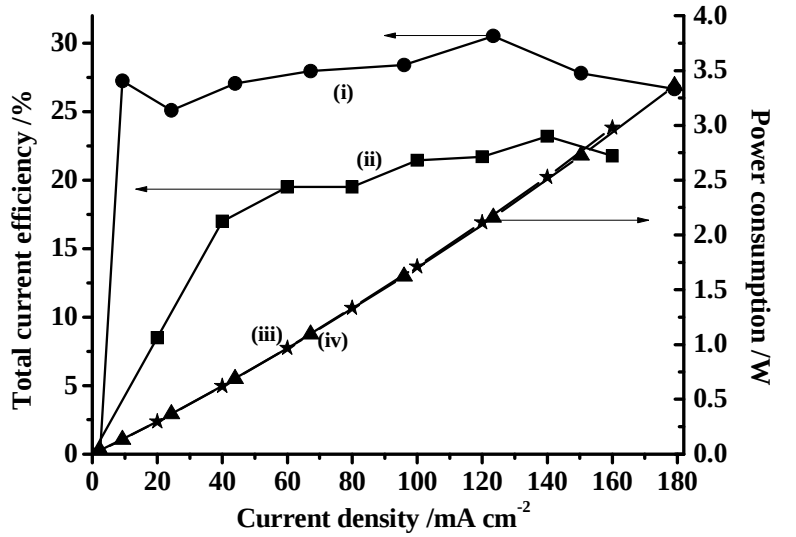

653

654 Figure 4(c)

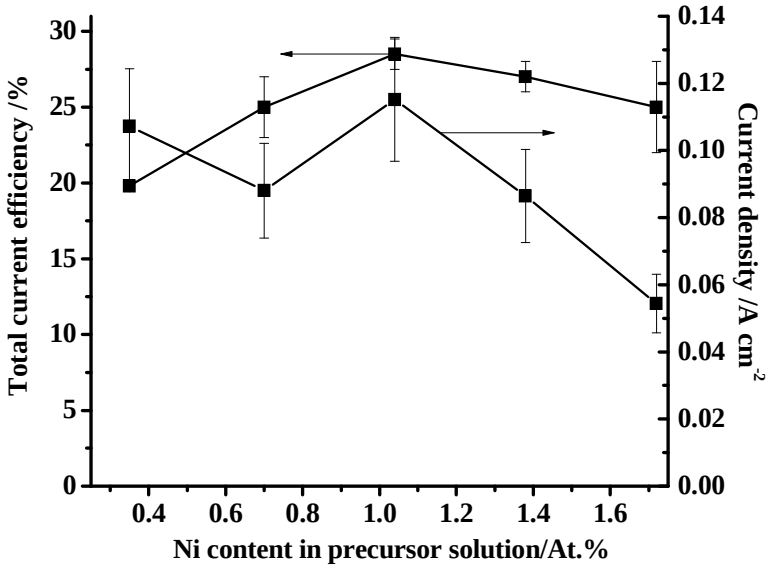

655

656 Figure 5(a)

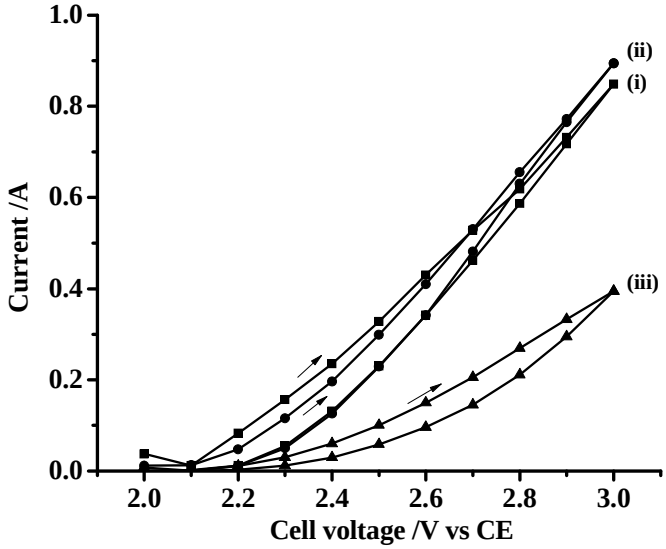

657

658 Figure 5(b)

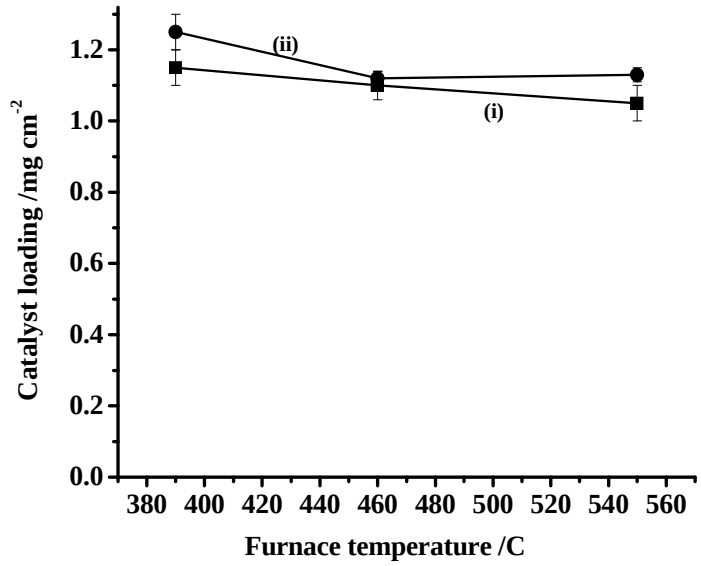

659

660 Figure 6(a)

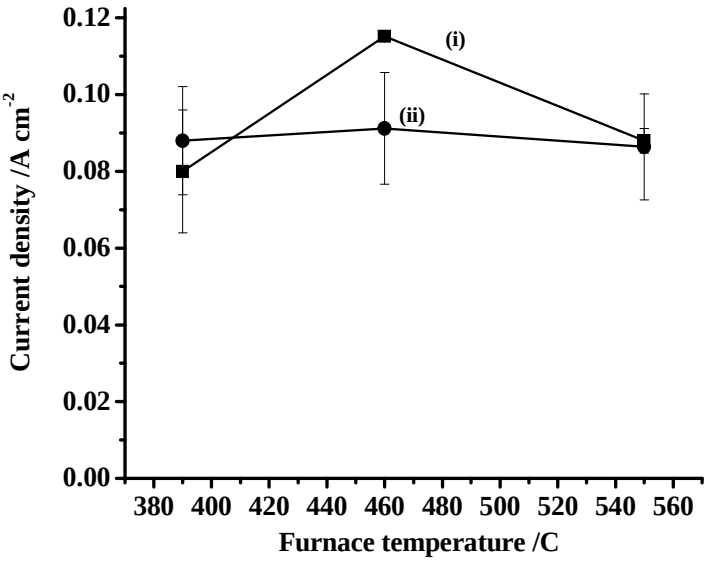

661

662 Figure 6(b)

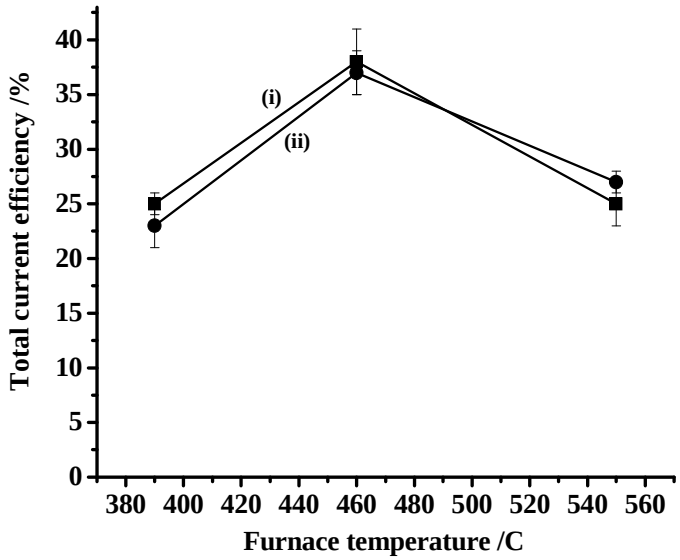

663

664 Figure 6(c)

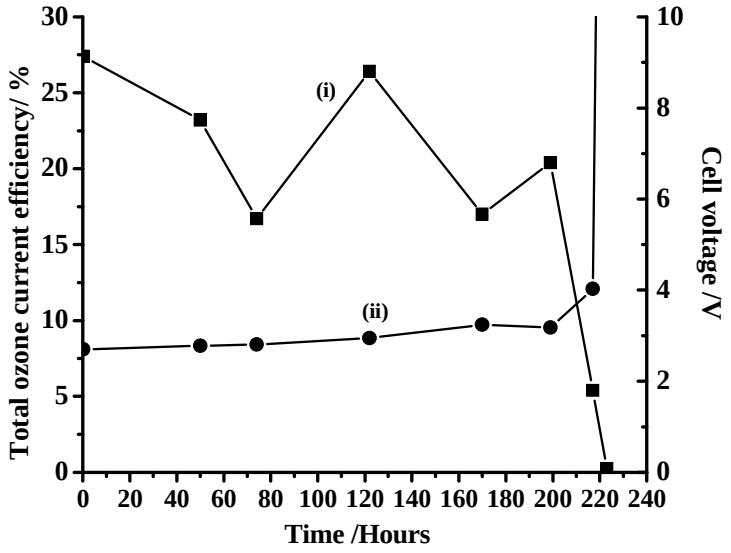

665

666 Figure 7

667

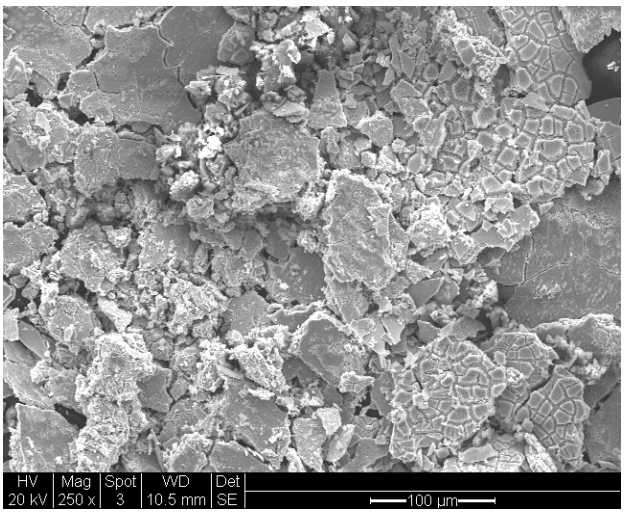

668

669 Figure 8

670